Form and Function of Clostridium thermocellum Biofilms

Alexandru Dumitrache, Gideon Wolfaardt, Grant Allen, Steven N. Liss and Lee R. Lynd
Appl. Environ. Microbiol. **2013, 79(1):231. DOI: 10.1128/AEM.02563-12.**
Published Ahead of Print 19 October 2012.

AEM
Journals.ASM.org

Form and Function of *Clostridium thermocellum* Biofilms

Alexandru Dumitrache,[a] Gideon Wolfaardt,[b] Grant Allen,[a] Steven N. Liss,[c] Lee R. Lynd[d]

Department of Chemical Engineering and Applied Chemistry, University of Toronto, Toronto, Ontario, Canada[a]; Department of Chemistry and Biology, Ryerson University, Toronto, Ontario, Canada, and Stellenbosch Institute for Advanced Study, Wallenberg Research Centre at Stellenbosch University, Stellenbosch, South Africa[b]; School of Environmental Studies and Department of Chemical Engineering, Queen's University, Kingston, Ontario, Canada[c]; Thayer School of Engineering, Department of Biological Sciences, Dartmouth College, Hanover, New Hampshire, USA[d]

The importance of bacterial adherence has been acknowledged in microbial lignocellulose conversion studies; however, few reports have described the function and structure of biofilms supported by cellulosic substrates. We investigated the organization, dynamic formation, and carbon flow associated with biofilms of the obligately anaerobic cellulolytic bacterium *Clostridium thermocellum* 27405. Using noninvasive, *in situ* fluorescence imaging, we showed biofilms capable of near complete substrate conversion with a characteristic monolayered cell structure without an extracellular polymeric matrix typically seen in biofilms. Cell division at the interface and terminal endospores appeared throughout all stages of biofilm growth. Using continuous-flow reactors with a rate of dilution (2 h^{-1}) 12-fold higher than the bacterium's maximum growth rate, we compared biofilm activity under low (44 g/liter) and high (202 g/liter) initial cellulose loading. The average hydrolysis rate was over 3-fold higher in the latter case, while the proportions of oligomeric cellulose hydrolysis products lost from the biofilm were 13.7% and 29.1% of the total substrate carbon hydrolyzed, respectively. Fermentative catabolism was comparable between the two cellulose loadings, with ca. 4% of metabolized sugar carbon being utilized for cell production, while 75.4% and 66.7% of the two cellulose loadings, respectively, were converted to primary carbon metabolites (ethanol, acetic acid, lactic acid, carbon dioxide). However, there was a notable difference in the ethanol-to-acetic acid ratio (g/g), measured to be 0.91 for the low cellulose loading and 0.41 for the high cellulose loading. The results suggest that substrate availability for cell attachment rather than biofilm colonization rates govern the efficiency of cellulose conversion.

Descriptions of microbial biofilms in the literature have most commonly featured inert surfaces and cells present within a matrix of extracellular polymeric material. *In situ* observations of biofilm samples have been made by many investigators in real time with the use of flow cells (1–3). Flow cells provide controlled growth conditions and allow nondestructive direct microscopic imaging of fully hydrated biofilms. Using flow cells, fine structural details have been revealed and physiological behavior has been observed by repeated observations over extended time periods.

Anaerobic biofilms have received much less study than aerobic biofilms, and very few reports to date have addressed the *in situ* observation of anaerobic, cellulolytic adherent species. Several studies have subjected slurry samples from batch fermentors to light and fluorescence microscopy, fluorescence *in situ* hybridization, and electron microscopy (4–6) and molecular and biochemical probing (7). Arguably, the first three methods have a destructive nature associated with sample preparation and can skew observation of the complexity of adherent structures, and the last two methods do not provide insights into colonization properties or spatial relationships. Studies of cellulolytic biofilms using nondestructive flow cells are few and are limited to mixed consortia enriched from landfill and the rumen (8, 9).

Clostridium thermocellum is among the most thoroughly described cellulolytic anaerobic bacteria. Although it has been understood for decades that *C. thermocellum* adheres to cellulosic substrates, the underlying mechanisms of attachment and the structural and behavioral characteristics of biofilms involving this organism are largely unknown.

C. thermocellum is a Gram-positive, strict anaerobe capable of hydrolyzing cellulose and hemicellulose while fermenting hexose sugar oligomers to ethanol, organic acids, carbon dioxide, and hydrogen gas. Its maximum specific growth rate on model crystalline cellulose substrates such as Avicel has been reported to be from 0.1 h^{-1} (10) to 0.16 h^{-1} (11) in batch culture and 0.16 h^{-1} in continuous culture (10). This bacterium is known to secrete membrane-bound cellulase enzymes complexes, termed cellulosomes, thought to be primarily responsible for its extracellular hydrolytic activity. Fermentation of cellulose by *C. thermocellum* is thought to involve extracellular hydrolysis into soluble oligomeric sugars which are then taken up by cells and undergo fermentative catabolism (12). The fraction of carbon passing through sessile and planktonic populations has not been evaluated for *C. thermocellum* or other cellulolytic anaerobes.

In this study, we sought to describe the characteristics of *Clostridium thermocellum* biofilms through nondisruptive *in situ*, high-resolution imaging and to utilize continuous-flow reactors with a high dilution rate and carbon mass balance analysis to evaluate the behavior of adhered cell populations separate from planktonic cells.

MATERIALS AND METHODS

Bacterial strains and chemicals. *Clostridium thermocellum* ATCC 27405 was kindly provided by Paul Weimer (University of Wisconsin) and maintained in batch cultures with RM medium (13) supplemented with

Received 19 August 2012 Accepted 16 October 2012
Published ahead of print 19 October 2012
Address correspondence to Gideon Wolfaardt, gwolfaar@ryerson.ca.
Supplemental material for this article may be found at http://dx.doi.org/10.1128/AEM.02563-12.

doi:10.1128/AEM.02563-12

Avicel PH-101 cellulose. All chemicals were reagent grade and were purchased from Sigma-Aldrich Co. (St. Louis, MO) or VWR International (PA) unless otherwise specified. Fluorescent stains were purchased from Life Technologies Inc. (ON, Canada). All gases were purchased from Linde Canada Ltd. (ON, Canada). Ultrapure water for medium preparation and analytical assays was obtained using a Milli-Q gradient system from EMD Millipore (ON, Canada) unless otherwise specified.

Culture media. Batch cultures of *C. thermocellum* were maintained in RM medium, which contained the following per liter of sterile water: 2 g CH_4N_2O, 2 g KH_2PO_4, 3 g K_2HPO_4, 2 g yeast extract, 1 g L-cysteine hydrochloride monohydrate, 0.002 g resazurin sodium salt, 0.2 g $MgCl_2 \cdot 6H_2O$, 0.05 g $CaCl_2 \cdot 2H_2O$, 0.0025 g $FeSO_4 \cdot 7H_2O$, and 5 g Avicel PH-101 as a source of cellulose. For continuous-flow-cell cultures used in imaging and effluent counts experiments, Avicel was omitted from the liquid medium and commercial household cotton was immobilized in the flow cell channels as the only cellulose source for growth. The medium was prepared for anaerobic work using a modified Hungate technique as previously described (14).

For the carbon mass balance experiments, a defined minimal-carbon (MC) medium was prepared with the least possible amount of noncellulosic carbon to ensure a very small background signal. The average total concentration of organic carbon measured in the medium, including traces from ultrapure water, was 7.3 mg/liter. The MC medium was a further modification of the low-carbon (LC) medium (15) with a yet lower carbon content and a composition optimized for continuous-flow-cell culturing. The medium was prepared as follows: the buffer system (2 g/liter NaH_2PO_4, 3.5 g/liter K_2HPO_4) and the nitrogen source [2 g/liter $(NH_4)_2SO_4$] were sterilized by autoclave (121°C for 20 min) in ultrapure water, and the medium vessel was then cooled under sparging with pure nitrogen gas; the sterile reducing agent (0.48 g/liter $Na_2S \cdot 9H_2O$) was added, and the medium was sparged with nitrogen for a minimum of 16 h. Sterile mixtures of minerals (0.2 g/liter $MgCl_2 \cdot 6H_2O$, 0.05 g/liter $CaCl_2 \cdot 2H_2O$, 0.02 g/liter $FeSO_4 \cdot 7H_2O$), vitamins (0.01 g/liter pyridoxamine dihydrochloride, 0.002 g/liter *p*-aminobenzoic acid, 0.001 g/liter biotin, 0.001 g/liter vitamin B_{12}, 0.002 g/liter thiamine, 0.0025 g/liter nicotinic acid, 0.00025 g/liter α-lipoic acid), and trace elements (0.00125 g/liter $MnCl_2 \cdot 4H_2O$, 0.0005 g/liter $ZnCl_2$, 0.000125 g/liter $CoCl_2 \cdot 6H_2O$, 0.000125 g/liter $NiCl_2 \cdot 6H_2O$, 0.000125 g/liter $CuSO_4 \cdot 5H_2O$, 0.000125 g/liter H_3BO_3, 0.000125 g/liter $Na_2MoO_4 \cdot 2H_2O$) were then added to complete the medium. Sterile nitrogen gas was continuously passed through the medium vessel while in use. Stocks of the separate solutions were prepared in nitrogen-filled serum vials at concentrations of 100× (reducing agent), 200× (minerals and vitamins), and 1,000× (trace elements) and sterilized by autoclave (reducing agent) or filtration through 0.2-μm-pore-size syringe filters (minerals, vitamins, and trace elements).

Imaging. Flow cells (3) with a modified chamber design (35 by 35 by 4 mm) were packed with cotton fibers as the sole cellulosic carbon source. The continuous-flow-cell system was assembled and sterilized in an anaerobic cabinet (type B vinyl anaerobic chamber; Coy Laboratory Products, MI), and the cultures were grown and stained *in situ* as detailed in the supplemental material. Cells were targeted with the green nucleic acid stain Syto 9, while cellulose fibers were visualized using the carbohydrate-binding lectin wheat germ agglutinin conjugated with red fluorescent tetramethyl rhodamine isothiocyanate (TRITC). Images were acquired *in situ* with a Nikon Eclipse 80i-C1 confocal scanning laser microscope (Nikon Instruments Inc., Canada) using a ×60 (numerical aperture [NA], 1.4) oil immersion objective and the EZ-C1 software package (Nikon Instruments Inc., Canada). Optical resolution was calculated at 178 nm using the Rayleigh formula, and *z* stacks were acquired at a 0.21-μm/pixel density and a 0.15-μm *z*-step size. Data manipulations (i.e., volume rendering, orthogonal projections) were carried out using the NIS-Elements software package (Nikon Instruments Inc., Canada). Syto 9 is a cyanine nucleic acid stain with low cell toxicity, and therefore, it is not recommended for use in time-resolved imaging. The cultures used in this study were discarded after staining and imaging.

Cell counts. Cotton-containing flow cells (55 by 3 by 3 mm) were inoculated with *C. thermocellum* (~10% of flow cell volume) at either the upstream or downstream port relative to the direction of medium flow. The different flow cell inoculation positions (upstream or downstream) represented two scenarios where the advance of biofilm growth to new cellulose regions was promoted or hindered by the flow.

Effluent samples were collected at 24-h intervals following inoculation for 5 and 6 days for upstream and downstream inoculation, respectively. Samples were immediately processed for total cell counts using an adapted epifluorescence direct enumeration technique (16, 17). Serial 10-fold dilutions were prepared in duplicate and stained with 4′,6-diamidino-2-phenylindole (DAPI; final concentration, 12.5 μg/ml), followed by incubation at room temperature, protected from light, for 20 min. Samples were then filtered through Nuclepore polycarbonate membrane filters (diameter, 25 mm; pore size, 0.2 μm; Whatman, VWR, Canada), thus uniformly distributing the sample content over 176.6 mm^2. Slides were immediately examined under fluorescence excitation on a Zeiss inverted fluorescence microscope (model Axiovert 200 M; Carl Zeiss Canada Ltd.) using oil immersion with a ×63 (NA, 1.4) Plan-Apochromat objective. A total of 30 randomly selected images were saved per sample, and only dilutions that contained between 20 and 200 cells per field were considered for counting. The Cell Counter plug-in of ImageJ software was used to sort cells into three groups, normal, dividing, and sporulated, each of which was counted. Cells were considered to be dividing when they exhibited a visible septum, in which case the joint bacteria were counted as two cells.

Continuous-flow reactors for carbon mass balance analysis. Cellulose filter paper (Whatman no. 1, with a minimum of 98% alpha-cellulose) was packed into reactors consisting of 5-ml, glass crimp-seal vials (VWR, ON, Canada) fitted with rubber stoppers (Bellco Glass Inc., NJ) and adapted with an inlet and outlet port. A nylon net filter (EMD Millipore, Canada) with a 20-μm pore size was placed in-line at the outlet port to prevent potential loss of filter paper fragments during fermentation. Masterflex Norprene tubing (Cole Palmer Inc., Canada) connected the reactor with the medium container at the inlet port and with a sterile, cooled (4°C), effluent collection vessel at the outlet port (see Fig. S1 in the supplemental material). To prevent contamination, the connection tubing and the reactor were sterilized for 2 h with 0.6% sodium hypochlorite and washed overnight with sterile water before each experiment. A 60°C sealed water bath continuously purged with nitrogen gas was used for reactor heating. Unidirectional flow from the medium container to the effluent vessel was maintained at 10 ml/h by a peristaltic pump (model 205S; Watson Marlow, Cornwall, England) which was placed after the water bath. The reactor was directly inoculated with *C. thermocellum* (~50% of the reactor volume) through the rubber crimp seal, and the medium flow was stopped for 1 h to allow substrate colonization. Flow was then resumed, and the inoculum excess was washed out into a separate container for 3 h to ensure no interference with the carbon analysis. To investigate carbon conversion exclusively through biofilm activity, we eliminated the potential formation of a resident planktonic population by the use of a relatively high dilution rate (2 h^{-1}), which is an order of magnitude higher than the bacterium's specific growth rate (≤0.16 h^{-1}). Two experimental conditions were investigated: low cellulose loading (LCL) and high cellulose loading (HCL). LCL experiments, repeated in triplicate, featured an average of 0.22 g cellulose in the reactor and had a duration of 4 days. HCL experiments, repeated in duplicate, featured approximately 1 g cellulose in the reactor and had a duration of 5 days. The carbon present at the end of fermentation in the solid, liquid, and gaseous phases was quantified as described below.

Solid-phase carbon. The mass of cellulose initially present (C_i) was determined by dry weight measurements of filter paper incubated for 3 h at 120°C. The mass of cellulose at the end of the experiment (C_f) was also determined by dry weight measurements following filtration on 934-AH borosilicate glass fiber filters (Sterlitech Corporation, WA).

Total biomass and cellulose in effluent samples were determined using

elemental carbon analysis (model TOC-V analyzer; Shimadzu Scientific Instruments, MD) against known standards, as follows. Unfiltered and filtered effluent samples were treated with NaOH (final concentration, 0.2 N) for 1 h at 50°C in sealed Falcon tubes (BD Bioscience, CA), conditions under which cellular biomass but not cellulose is digested (18). The posttreatment mixtures were filtered to remove undigested residual cellulose particles, and the total organic carbon (TOC) content was determined. The difference between unfiltered and filtered effluent TOC ($TOC_{e,unfiltered}$ and $TOC_{e,filtered}$, respectively) was interpreted as effluent biomass (B_e). The effluent cellulose content (C_e) was calculated on the basis of a carbon balance, as follows:

$$C_e = TOC_{e,unfiltered} - TOC_{e,filtered} - B_e \quad (1)$$

All filtrations in this procedure used 0.2-μm-pore-size hydrophilic polyvinylidene difluoride Target syringe filters (Fisher Scientific, ON, Canada) prewashed with 30 ml of ultrapure water to ensure no trace carbon loss or gain. Elemental analysis with the TOC-V analyzer measures total carbon (TC) and inorganic carbon (IC) by wet oxidation coupled with nondispersive infrared detection, while TOC concentrations are calculated by subtracting IC from TC values. Biofilm left on residual cellulose (C_f) in the reactor at the end of culture growth was considered to have no meaningful impact on the total carbon balance, as most of the cell mass was already released in the effluent following the solid substrate breakdown and disappearance from the reactor.

Gas-phase carbon. The spargeable carbon dioxide [$CO_{2(g)}$] formed during the fermentation was removed from the effluent by continuous sparging of the effluent vessel with nitrogen gas at a flow rate of 20 ml/min. The concentration of CO_2 in the resulting stream was measured in real time with an infrared gas analyzer (model LI-820 CO_2 analyzer; LI-COR Biosciences, Lincoln, NE), which was calibrated against known standards. The total amount of spargeable CO_2 was calculated by integrating the flow rate-weighted concentration measurements over time using the trapezoidal rule (19).

Liquid-phase carbon. The noncellulosic carbon in the culture medium, referred to as baseline medium carbon, was measured by TOC ($M_{baseline}$) and IC analysis; however, due to continuous sparging during preparation, the IC content was virtually undetectable.

Carbonates and dissolved CO_2, i.e., aqueous CO_2 [$CO_{2(aq)}$], were measured by IC analysis as a pooled value in filtered effluent samples at the end of culture growth and represented the fermentation CO_2 that remained trapped in the aqueous phase.

Hydrolysis products lost from the biofilm ($Hydr_{loss}$) were measured in filtered effluent samples using the phenol-sulfuric acid assay (20) against glucose standards.

Ethanol, acetic acid, lactic acid, formic acid, glucose, and cellobiose were measured in filtered effluent samples using high-pressure liquid chromatography (HPLC) against known concentrations of standards in the range of 0.5 mM to 20 mM. One-milliliter aliquots were acidified with 10 μl of 37% (wt/wt) HCl and centrifuged for 5 min at 10,000 × *g*. The supernatants were analyzed with a Bio-Rad HPX-87H column, operated at 60°C and 0.6 ml/min with a 5 mM H_2SO_4 mobile phase, using refractive index and UV absorbance (λ = 210 nm) detection. Ethanol in the low concentration range was also determined using an enzymatic ethanol assay kit (Megazyme International, Wicklow, Ireland) according to the supplier's protocol.

Carbon balance calculations. Hydrolyzed cellulose ($C_{hydrolyzed}$) was calculated on the basis of the following:

$$C_{hydrolyzed} = C_i - C_f - C_e \quad (2)$$

The average rate of hydrolysis was normalized to incubation time.

Metabolized cellulose ($C_{metabolized}$) was calculated on the basis of equation 3:

$$C_{metabolized} = C_i - C_f - C_e - Hydr_{loss} \quad (3)$$

The total cellulosic carbon accounted for (percent recovery) was calculated using equation 4:

$$\text{percent recovery} = \{[TOC_{e,unfiltered} + C_f + CO_{2(g)} + CO_{2(aq)} - M_{baseline}]/C_i\} \times 100 \quad (4)$$

Statistical analysis. Where appropriate, statistical analysis was performed using the MyStat software package. The equality of variances between two samples was analyzed using the *F* test at the 95% confidence level. The equality of means was analyzed using an unpaired two-sample *t* test at the 95% confidence level, and the *P* value was calculated using separate or pooled variances on the basis of the results of the *F* test.

RESULTS

Biofilm structural characterization. Growth in flow cells appeared at the inoculation site, with subsequent progression to adjacent uncolonized surfaces and gradual depletion of the solid substratum. Biofilms were observed at various degrees of cellulose colonization, from scattered cell groups to regions with very high cell density (Fig. 1A to C); however, they were invariably represented primarily by a single layer of cells. Biofilm features were documented at approximately 200-nm resolution: vegetative cells lay along the substrate with an orientation parallel to that of carbon fibers and over time formed progressively longer chains. As the biofilm density increased, cells increasingly appeared with a perpendicular orientation relative to the axis of the cotton fibers. Numerous terminal endospores were observed, with spores generally forming at the end of cells away from the cellulose surface and in regions of high cell density. Highly elongated sporangia were occasionally observed at the solid-liquid interface (Fig. 1D). On further inspection, biofilms closely followed the cellulose topography, with each cell maintaining direct contact with the substrate. A cell-substrate gap could not be observed at the limit of detection, equal to the equivalent pixel size of scanned images, about 210 nm (Fig. 2).

Substrate colonization and cell detachment. To investigate cell detachment with respect to substrate surface area limitations, separate flow cells were inoculated at the influent port (i.e., upstream inoculation), where biofilm expansion benefited from the hydrodynamic flow, or at the effluent port (i.e., downstream inoculation), where biofilms had to colonize new regions against the liquid flow. As expected, upstream inoculation resulted in faster biofilm spread and substrate degradation, with the average cell elution being 2-fold higher. The difference was statistically significant at the 95% confidence level ($P = 0.014$, in a two-sample *t* test with unequal variances). Bacterial cells detached from the cellulose interface during all stages of biofilm development (with respect to colonization density), and there appeared to be no discernible preference of cell life cycle stage for detachment (Fig. 1D, white arrows). Dividing and sporulating cells represented 11% ± 3% and 5% ± 3% of the total population of detached cells, respectively, as determined by microscopic examination.

Cell detachment peaked at day 5 for the upstream-inoculated flow cell, which marked the complete dissolution of the substrate, while for downstream inoculation, the biofilm front reached the midpoint of the flow channel after 6 days with a modest increase in cell detachment (Fig. 3A). The ratio between sporulated and actively dividing cells measured in the effluent feed was plotted for the two treatments over a 5-day incubation period (Fig. 3B), and opposite trends were observed. Upstream-inoculated flow cells initially exhibited a high incidence of dividing cells but with the fraction of sporulating cells gradually increasing. Downstream-inoculated flow cells initially exhibited a high incidence of sporulated cells which declined over time.

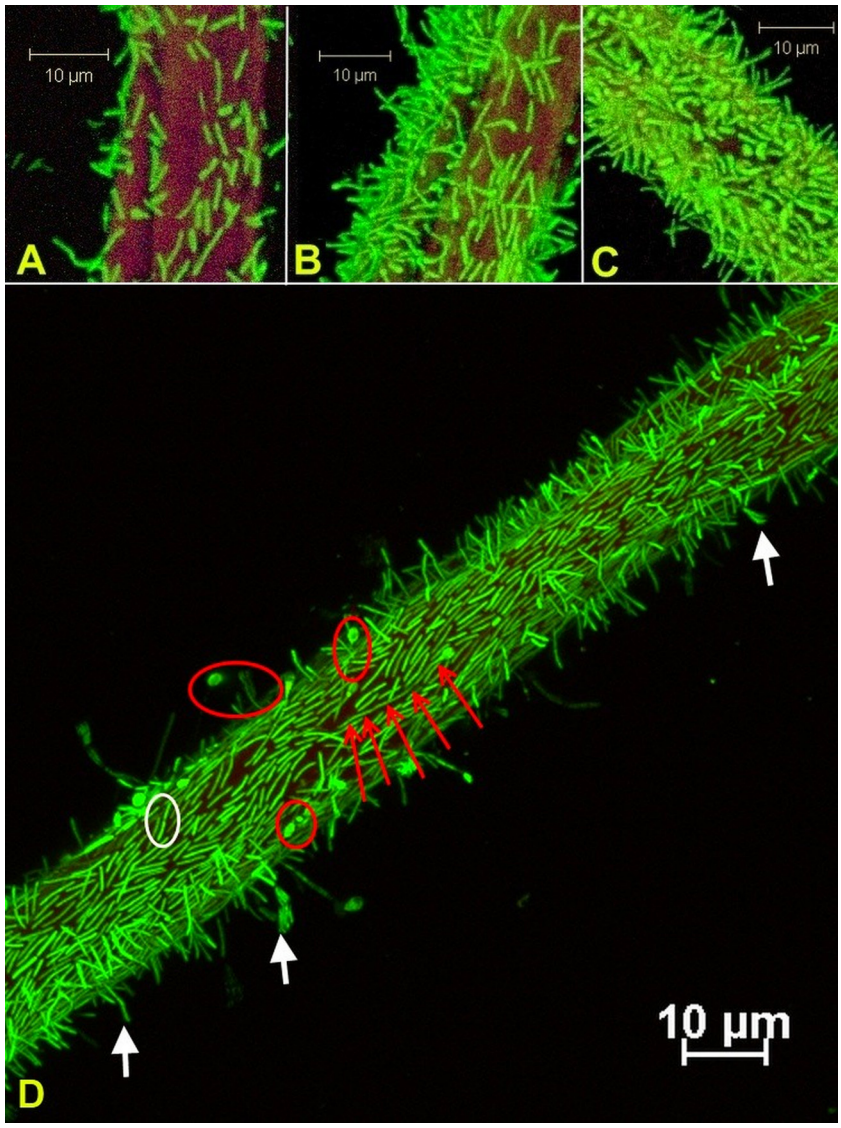

FIG 1 (A to C) Confocal laser scanning micrographs of *Clostridium thermocellum* 27405 biofilms on cellulose cotton fibers show substrate colonization with various degrees of cell density after approximately 48 h of incubation; before total substrate colonization occurred, the density on the fibers decreased by imaging further from the inoculation region. (D) A monolayer of cells was the defining characteristic of fresh and mature biofilms, while typical terminal endospores attached at the nonsporulating end (red circles), cell division occurred at the interface (white circles), and highly elongated sporangia (red arrows) and detaching cells (white arrows) were frequently observed. Cells were stained with Syto 9; cellulose fibers were stained with wheat germ agglutinin-TRITC.

Carbon flow in *C. thermocellum* biofilms. Substrate loading and medium consumption were compared between the typical batch fermentor (10) and the continuous-flow-cell reactor used in this study (Table 1). Culture performance was also compared between reactors with lower (LCL) and higher (HCL) starting cellulose concentrations. In the latter, medium consumption was low and the average rate of hydrolysis was considerably higher (Table 1); however, the percentage of hydrolysate lost from the biofilm-substrate interface also significantly increased.

Carbon partitioning within the two experimental treatments is summarized in Table 2. On average, between measurements of gas, liquid, and solid product fractions, 91% of the initial carbon was accounted for. Statistically significant differences in hydrolysate retention and acetate production were found. The average ethanol-to-acetic acid ratio was 0.91 g/g (or 1.18 mol/mol) in LCL trials and 0.41 g/g (or 0.53 mol/mol) in the HCL treatments. Formic acid above the 0.2 mM limit of detection was not found by HPLC analysis.

DISCUSSION

Biofilm structure and growth. The development of *C. thermocellum* biofilms on cellulose, as observed in this study, proceeds from initial colonization and localized patches of loosely packed adherent cells to complete coverage of the available cellulosic surface. Scattered cells start dividing at the interface (much like colonies on a plate develop) to form a confluent monolayer along the substratum; however, biofilm maturation was also found to be coupled with continuous recruitment of cells from the aqueous suspension, as previously described for biofilms growing on inert surfaces (21). Cell density increases along the adherent surface,

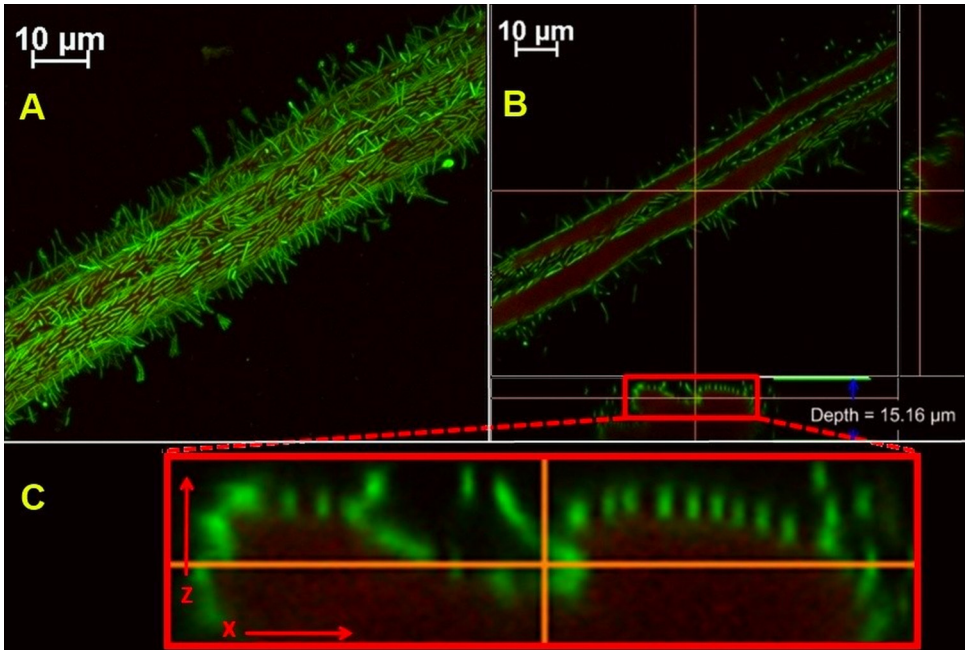

FIG 2 (A) *Clostridium thermocellum* biofilm on cotton fiber shown in the *x-y* plane of a reconstituted volume render. (B) Optical sectioning along the cellulose in the *x-y* plane, and vertical sectioning (i.e., orthogonal projections) along the indicated red lines showed biofilms that were closely lining the adhesion interface. (C) Vertical sectioning along the *x-z* plane is enlarged to reveal no visible cell-substrate gap. The original image was scanned at 0.21 μm/pixel, the *z*-step size was 0.15 μm, and the optical resolution was calculated to be 178 nm using the Rayleigh formula. Cells stained with Syto 9; cellulose was stained with wheat germ agglutinin-TRITC.

and while cells have multiple orientations toward the substrate, they do not overlap in multiple layers. This trend is of relevance with respect to the ultimate binding affinity toward their carbon source; this cellulolytic organism requires close proximity to the substrate for efficient utilization, which suggests that carbohydrate capture in the bulk aqueous phase is not the preferred mode. Considering that adherent cell populations were found to be the most strongly correlated to first-order rates of cellulose hydrolysis (22) in leachate and rumen consortia, it remains to be seen how the *C. thermocellum* cell distribution would be affected in complex and potentially competitive multispecies biofilms.

The simplicity in observed biofilm structure is emphasized by the lack of a typical biofilm matrix. We showed in previous work that carbohydrate-targeted staining (i.e., commonly used lectins) failed to reveal an extracellular polymeric substance (EPS) interconnecting adherent cells. However, the concanavalin A lectin, with primary affinity for α-glucose and α-mannose, was found to bind the surface of cells, which points to a glycocalyx-like secretion containing these sugar residues (14).

Close interaction between the bacterium and the substrate presents several advantages, in particular, cellulolytic enzyme concentration at the boundary layer and fast capture of oligomeric hydrolysis products. In fact, protuberances of cellulosome clusters embedded in the cell membrane were theorized to mediate the uptake of sugars directly from the hydrolysis site (23). In contrast, an absent extracellular matrix and the inability to grow in thickness raises the question whether these biofilms possess the basic characteristics of classical adherent populations, including protection from predation by protozoa, bacteriophage or protease attack, adverse environmental conditions (e.g., desiccation), and sequestration of nutrients at the interface in the EPS lattice. It appears that *C. thermocellum* biofilms are structurally and functionally distinguishable, as there is little evidence describing other monolayered biofilms in current literature, although it is recognized that most studies to date have focused on attachment to inert surfaces. A relatively unique trait of these cellulolytic biofilms is their transient nature. The substrate is the prime carbon source and the support platform, which is eroded by cellulases in a stepwise progression (24) until the biofilm collapses and cells revert back to the planktonic stage. Therefore, while classical biofilms are generally described to be a form of microbial survival and persistence, the unique cellulolytic monolayers of *C. thermocellum* are best understood to be the bacterium's functional adaptation to a recalcitrant substrate.

Cell adhesion and detachment. Cellulolytic species bind to cellulose through a series of proposed mechanisms, most notably, the carbohydrate binding domains (CBDs) in the cellulase systems, cellulose binding proteins associated with the cell envelope, secreted glycoproteins (i.e., glycocalyx) (25), or fimbria-like mediation (26). The mechanisms involved in *C. thermocellum* adhesion are not clearly defined; however, a combination of CBDs and cell surface glycoproteins is expected to be involved. In related strain JW20, strong adhesion to cellulose and, to a much lower extent, to hemicelluloses was observed to occur through mucopolysaccharide-containing fibrous material (27), which was later described in strain 27405 to be cellulosome-rich protuberances (23). However, in JW20, attachment to cellulose in batch cultures was reported to be temporary, primarily during mid-logarithmic phase, was inhibited by additions of small amounts of soluble sugars, and was not affected by supplements of fermentation end products, thus suggesting that cell adhesion is an active regulatory function for carbon utilization. Contrary to this pattern, we ob-

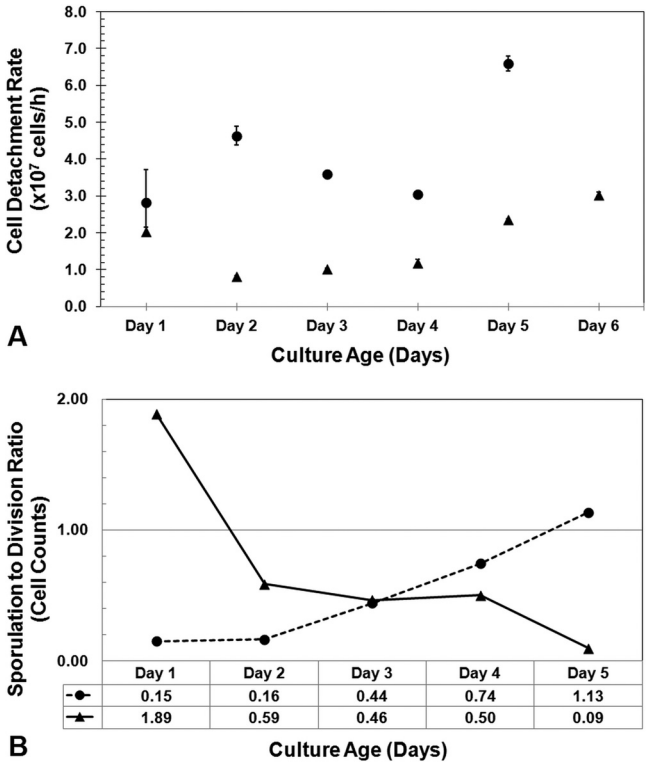

FIG 3 (A) Detachment rates of biofilm-generated cells were compared for tubular flow channels packed with cellulose that were inoculated at the upstream (●) or the downstream (▲) port relative to the direction of medium flow. Hydrodynamic forces therefore promote or obstruct further substrate colonization. (B) Effluents were ordered on the basis of life cycle morphology, and the ratio of sporulating cells to actively dividing cells was used to compare the colonization intensity in the upstream (●) or the downstream (▲) inoculated flow cells. A higher ratio indicated predominantly dense biofilms forming on cotton fibers as a consequence of surface area limitations.

served strain 27405 to exhibit very strong cellulose binding throughout complete hydrolysis cycles with or without the presence of labile carbohydrates in the medium flow. In strain 27405, previous estimates place the cell-to-substrate distance at over 500 nm (4); however, our analysis of optical sections through *in situ* biofilms points to a much smaller gap of under 210 nm. It remains to be seen how this impacts mass transfer properties within the thin liquid gap under the cells, especially with respect to biomolecule diffusion between the substrate and the cell surface or the fast-flowing bulk liquid phase.

TABLE 1 Characteristics of continuous-flow cultures of *C. thermocellum* biofilms operated at a dilution rate of 2 h^{-1}[a]

Characteristic	Low carbon load	High carbon load
Initial amt of cellulose (g)	0.22	1.01
Cellulose concn normalized to reactor vol (g/liter)	44	202
Increase over batch fermentor[b] concn (fold)	9	40
Liquid medium consumption/g cellulose (liters)	3.4	0.86
Increase over batch fermentor[b] medium usage (fold)	17	4.3
Average rate of cellulose hydrolysis (g h^{-1})	0.002	0.007
Average culture age (h)	92	117

[a] The cellulose concentration was normalized to the reactor volume or the total amount of culture medium used in low- and high-load experiments and compared to typical values for batch fermentors. The overall rate of hydrolysis is normalized to the incubation time.
[b] Typical batch fermentors used in microbial cellulose conversion studies utilize 5 g of substrate per liter of culture medium.

TABLE 2 Summary of carbon mass balance analysis for continuous-flow cultures of *C. thermocellum* grown on cellulose filter paper[a]

Parameter	% (g carbon/g carbon)	
	LCL	HCL
Normalized to initial cellulose		
Residual	13.0	19.9
In flow cell	6.6	14.9
In effluent	6.5	5.0
Hydrolyzed	87.0	80.2
Normalized to hydrolyzed cellulose		
Hydrolysate loss	13.7[b]	29.1[b]
Glucose	ND	0.0
Cellobiose	ND	9.4
Metabolized cellulose	86.3[b]	70.9[b]
Normalized to metabolized cellulose		
Biomass	4.0	3.6
Carbon dioxide	17.9	14.3
Spargeable CO_2	17.4	13.6
Carbonates and dissolved CO_2	0.5	0.7
$C_2 + C_3$ metabolites	57.5	52.4
Ethanol	23.6	14.7
Acetic acid	19.9[b]	28.1[b]
Lactic acid	14.0	9.7

[a] Two treatments for different amounts of starting cellulose carbon (98.3 mg for LCL and 448.1 mg for HCL) were compared. The reactor dilution rate was 2 h^{-1}. ND, theoretically not detectable by HPLC, on the basis of the proportion of total hydrolysate loss.
[b] Statistically significant difference between means at the 95% confidence level using an unpaired two-sample *t* test.

Detachment occurs during all stages of biofilm growth, much like in aerobic biofilms developing on inert materials (28). However, due to the transient nature of cellulolytic cultures, substrate collapse is followed by the sharp increase in the release of cells to the bulk liquid phase (7).

The correlation between cell life cycle events (i.e., division, sporulation) and detachment from cellulosic substrates has not been described. Hydrodynamic forces are likely an important contributing factor, and therefore, it is assumed that indiscriminate detachment occurs in the case of all cell types. Coupled with our consistent observations of terminal endospores on densely colonized substrates and continuous cell division, the relative proportion of these two forms in effluent counts may be an indicator of colonization density and therefore of available attachment surfaces. Higher division rates would indicate unrestrained biofilm growth, while increased sporulation would signal substrate limitations. This is supported by the contrasting trends in the tested scenarios where medium flow through flow channels packed with cellulose was used to drive or to impede the biofilm's advance to new attachment sites (Fig. 3B).

Sporulation. In batch cultures of strain JW20, sporulation occurs in the late logarithmic phase as a response to lowered pH values, and as indicated by Wiegel and Dykstra, sporangia with swollen termini bind with the nonsporulating end at the attach-

ment substrate and could represent the entire cell population (27). Fully developed spores exhibit heat resistance of up to 2 h at 100°C, and dependent upon heat activation treatment, they require between 10 and 30 h to germinate. For strain LQRI, the decimal reduction time at 121°C (i.e., 90% kill efficiency of spores) is 0.5 min; however, heat resistance can vary in proportion to the spore cortex volume (29). According to these accounts, sporulation is a survival adaptation in environments with periodical temperature elevations (e.g., sun exposure), with the spore cortex acting as a regulatory organelle preventing dehydration that may be induced by the accumulation of ethanol and organic acids (30). More recent discoveries into the mechanisms that trigger spore formation in *Clostridium acetobutylicum* might present a good parallel to those for the *C. thermocellum* species. Genetic mutations in an accessory gene regulator (*agrBDCA*) system that controls quorum sensing (QS) through auto-induced peptide (AIP) secretion have been linked to spore formation in *C. acetobutylicum* (31). Quorum sensing allows bacteria to regulate gene expression in relation to cell population densities, and there is evidence that cell-to-cell communication systems are widely distributed within *Clostridium* spp. (32). Furthermore, an *agrC* gene has been identified in the genome of a *C. thermocellum* environment isolate (33), but it is yet unknown if the species-specific AIP QS is functional or controlled by the *agr* operon.

Lastly, one account links sporulation initiation with the peak endoglucanase transcription levels which occur during the transition to stationary phase and, hence, toward cessation of growth in batch cultures of *C. thermocellum* (34). This is supported by the identification of two promoter sequences upstream of endoglucanase genes *celA* and *celD* that have high homology with the σ^D promoter of sporulation transcription factors in *B. subtilis*.

Our *in vivo* observations of attached terminal endospores in high-density areas are of particular importance because these biofilms, arguably, do not suffer from metabolite accumulation, lowered pH, temperature variations, or exposure to oxygen, and the cultures do not have a typical stationary phase with a general cessation of growth. There is no doubt that these are factors that may contribute, alone or in combinations, to the stress-survival response of this bacterium; however, it appears that sporulation also acts as a response to facilitate proliferation.

High endoglucanase transcription may also signal an increase in solubilized sugar uptake and a reversal to a dormant state for energy conservation. Alternatively, in congested monolayers, intraspecies cell-to-cell signaling might trigger reversal to the resistant form in preparation for translocation to new cellulosic substrates. Overall, since spores do not contribute to fermentative catabolism, a deeper understanding of their regulation is needed to delineate the benefits that they may bring to culture growth and cellulose conversion.

Biofilm activity and carbon flow. A direct comparison of substrate hydrolysis efficiency with commonly used batch fermentors is difficult to make. Studies described in the literature typically use a cellulose load of 5 g per liter of liquid medium. In continuous flow, we employed 9-fold and 40-fold increased loads; however, due to the high dilution rate, these reactors used up to 17-fold and 4.3-fold more medium per gram of cellulose, respectively. Considering these differences, 4-day (LCL) and 5-day (HCL) cycles for the hydrolysis of 87% and 80% of the cellulose, respectively, appear to be within the normal efficiency for *C. thermocellum*. Given sufficient time in our experiments, cellulose breakdown reached near completion, demonstrating the biofilms' proficiency at total substrate degradation without a contribution from a cellulolytic planktonic cell population.

An important consideration is the rather large difference in the average rate of hydrolysis for the two cellulose loadings (Table 1). Considering the equal cultivation conditions and, therefore, similar biofilm growth and the fact that cellulose hydrolysis is a surface reaction, it is evident that hydrolysis rates are dependent on the total surface area available for microbial attack. This relationship has been well established in the case of pure enzymatic breakdown of cellulosic feedstock (35, 36). Furthermore, the comparable fermentative catabolism in the two treatments (Table 2), indicative of similarly active cell populations, suggests that at these substrate loadings, the rate of biofilm colonization was not a primary limiting step for cellulose breakdown. An in-depth analysis of these correlations is the subject of ongoing research.

A point of contention in the batch fermentation literature remains the inability to accurately determine the portion of soluble oligomers that escapes capture by attached cells to dissolve into the bulk liquid phase, where the oligomers sustain the growth of planktonic populations. Recent endpoint analysis of Avicel-grown *C. thermocellum* found very small amounts of soluble xylan and glucan, with degrees of polymerization (d.p.) no larger than 3 to 4, and no glucose or cellobiose in the fermentation broth (19). An important contribution of our high-flow reactors to carbon balance analysis is the capacity to measure total hydrolysate loss from the reactive interface without the constraint of subsequent sugar consumption by the increasingly large planktonic population that is prevalent in batch systems. In contrast, we report that an average of 13.7% (LCL) and 29.1% (HCL) of hydrolyzed sugar is lost to the bulk liquid phase, with cellobiose accounting for up to a third of it, while no glucose is present. Glucose has been shown to elicit a 4-fold higher cell maintenance energy than cellobiose (37), with *C. thermocellum* known to internalize oligomers as large as cellopentaose (38) and to gain energetic growth benefits with increasing chain length (12); therefore, the loss of hydrolysate with higher d.p. is not surprising.

The loss of sugar from the biofilm layer can be expected from an ecological perspective, as planktonic cell growth is to a large degree dependent on the diffusion of labile carbon from an insoluble substrate, especially in environmental cellulolytic consortia, where the free cells can account for up to 75% of total biomass (18). However, the substantial increase in hydrolysate loss with higher concentrations of initial cellulose is rather surprising. This is the first demonstration of this phenomenon, and further analyses are required to understand its underlying mechanisms, be it hydrolysate diffusion in the cell-substrate interface or the potential changes in cellodextrin transport across membranes. Alternatively, a comparison can be made to the ruminal bacterium *Fibrobacter succinogenes*, which secretes cellobiose and higher cellodextrins into the culture medium (39) through the reversible activity of intracellular phosphorylases (CbP and CdP), also present in *C. thermocellum*. These enzymes have an *in vitro* equilibrium which favors synthesis of longer oligomers from simpler saccharides (40). Interestingly, this conversion is observed in nongrowing cell suspensions but not in planktonic populations that can utilize cellodextrins for division (39). It is reasonable, then, to consider intracellular polymerization and secretion to be an equilibrium function between sugar retention and cellular metabolism needs. Conceivably, *C. thermocellum* biofilms with overall similar

metabolic performance (Table 2) and access to different amounts of solubilized sugar would balance their excess by the release of carbon to the bulk liquid phase.

In order to analyze the metabolic activity of biofilms under low and high carbon loads, the carbon balance of primary metabolites and cellular biomass was normalized to the amount of consumed rather than hydrolyzed cellulose. Under these conditions, cell mass production was proportionally equivalent between the two treatments at about 4% of metabolized substrate; however, this figure is roughly three times lower than the biomass production reported in batch fermentors (19), where a resident population of nonadherent cells is maintained. In related strain JW20, free cells accounting for up to 50% of total biomass were observed during all stages of growth (27).

The primary carbon metabolites measured were ethanol, acetic acid, lactic acid, and carbon dioxide. A significant difference was observed only for acetic acid production, which increased under higher carbon loads. A direct comparison to the metabolite profiles of cultures grown under stationary conditions is not practical primarily due to differences with respect to the high dilution and removal of end products and of nonadherent cells, which potentially utilize different metabolic pathways. Metabolism by stationary and low-dilution *C. thermocellum* cultures is well documented; and large variations are observed under various conditions, such as conditions that include mixing and hydrogen removal (41, 42); conditions in which the medium composition, pH, and substrate loading vary (11, 43, 44); as well as conditions that include the addition of end products, changes in bacterium growth rates, or reactor pressurization with gases (40, 45, 46). Our analysis may serve as a reference for carbon conversion exclusively through biofilm activity under various initial carbon loading.

Lastly, one important observation warrants consideration: the average ethanol-to-acetic acid ratio (0.91 g/g) in LCL trials fell within reported values (0.88 to 1.31 g/g) for cellulose fermentation in reactors with much lower dilution rates (0.05 to 0.17 h^{-1}) (10); however, this ratio was notably lower (0.41 g/g) in the HCL trials, where acetic acid production was favored. It appears that maximizing carbon loads may present the benefit of overall faster substrate breakdown but at a higher loss of valuable soluble sugars and a shift away from ethanol production.

Conclusions. On the basis of the premise that fundamental features of cellulolytic biofilms have been largely unexplored in the literature, our investigation marks the first attempt at describing the unique characteristics of transient *Clostridium thermocellum* biofilms. Furthermore, using continuous-flow reactors to determine carbon partitioning within these cultures, we demonstrate the central role that biofilms play in the overall utilization of cellulosic substrates. To this end, biofilms can be regarded as important catalytic units of cellulose fermentation; therefore, increasing their mass and surface exposure may hold several advantages; alternatively, each adherent cell can be seen to be a functional biological reactor where the fluid transport characteristics in its microenvironment regulate the performance.

ACKNOWLEDGMENTS

The research presented here has been supported by funding grants from Mascoma Corporation (MA), the Agricultural Biorefinery Innovation Network, Genome Canada, and the Natural Sciences and Engineering Research Council of Canada.

REFERENCES

1. **Lawrence JR, Korber DR, Hoyle BD, Costerton JW, Caldwell DE.** 1991. Optical sectioning of microbial biofilms. J. Bacteriol. **173**:6558–6567.
2. **Palmer RJ, Jr.** 1999. Microscopy flowcells: perfusion chambers for real time study of biofilms. Methods Enzymol. **310**:160–166.
3. **Wolfaardt GM, Lawrence JR, Robarts RD, Caldwell SJ, Caldwell DE.** 1994. Multicellular organization in a degradative biofilm community. Appl. Environ. Microbiol. **60**:434–446.
4. **Bayer EA, Shimon LJW, Shoham Y, Lamed R.** 1998. Cellulosomes—structure and ultrastructure. J. Struct. Biol. **124**:221–234.
5. **O'Sullivan CA, Burrell PC, Clarke WP, Blackall LL.** 2005. Structure of a cellulose degrading bacterial community during anaerobic digestion. Biotechnol. Bioeng. **92**:871–878.
6. **Syutsubo K, Nagaya Y, Sakai S, Miya A.** 2005. Behavior of cellulose-degrading bacteria in thermophilic anaerobic digestion process. Water Sci. Technol. **52**:79–84.
7. **Gelhaye E, Petitdemange H, Gay R.** 1992. Characteristics of cellulose colonization by a mesophilic, cellulolytic *Clostridium* (strain C401). Res. Microbiol. **143**:891–895.
8. **Jones LR, Watson-Craik IA, Senior E.** 1997. Image analysis for the study of the development of anaerobic biofilms on materials characteristic of landfilled refuse. Water Sci. Technol. **36**:485–492.
9. **O'Sullivan CA, Burrell PC, Pasmore M, Clarke WP, Blackall LL.** 2009. Application of flowcell technology for monitoring biofilm development and cellulose degradation in leachate and rumen systems. Bioresour. Technol. **100**:492–496.
10. **Lynd LR, Grethlein HE, Wolkin RH.** 1989. Fermentation of cellulosic substrates in batch and continuous culture by *Clostridium thermocellum*. Appl. Environ. Microbiol. **55**:3131–3139.
11. **Islam R, Cicek N, Sparling R, Levin D.** 2009. Influence of initial cellulose concentration on the carbon flow distribution during batch fermentation by *Clostridium thermocellum* ATCC 27405. Appl. Microbiol. Biotechnol. **82**:141–148.
12. **Zhang YP, Lynd LR.** 2005. Cellulose utilization by *Clostridium thermocellum*: bioenergetics and hydrolysis product assimilation. Proc. Natl. Acad. Sci. U. S. A. **102**:7321–7325.
13. **Ozkan M, Desai SG, Zhang Y, Stevenson DM, Beane J, White EA, Guerinot ML, Lynd LR.** 2001. Characterization of 13 newly isolated strains of anaerobic, cellulolytic, thermophilic bacteria. J. Ind. Microbiol. Biotechnol. **27**:275–280.
14. **Dumitrache A, Wolfaardt GM, Lynd LR.** 2010. Surface microbiology of cellulolytic bacteria, p 634–643. *In* Baltz RH, Davies JE, Demain AL (ed), Manual of industrial microbiology and biotechnology, 3rd ed. ASM Press, Washington, DC.
15. **Holwerda EK, Hirst KD, Lynd LR.** 2012. A defined growth medium with very low background carbon for culturing *Clostridium thermocellum*. J. Ind. Microbiol. Biotechnol. **39**:943–947.
16. **Kepner RL, Jr, Pratt JR.** 1994. Use of fluorochromes for direct enumeration of total bacteria in environmental samples: past and present. Microbiol. Rev. **58**:603–615.
17. **Massana R, Gasol JM, Bjørnsen PK, Blackburn N, Hagström A, Hietanen S, Hygum BH, Kuparinen J, Pedrós-Alió C.** 1997. Measurement of bacterial size via image analysis of epifluorescence preparations: description of an inexpensive system and solutions to some of the most common problems. Sci. Mar. **61**:397–407.
18. **Jensen PD, Hardin MT, Clarke WP.** 2008. Measurement and quantification of sessile and planktonic microbial populations during the anaerobic digestion of cellulose. Water Sci. Technol. **57**:465–469.
19. **Ellis LD, Holwerda EK, Hogsett D, Rogers S, Shao X, Tschaplinski T, Thorne P, Lynd LR.** 2012. Closing the carbon balance for fermentation by *Clostridium thermocellum* (ATCC 27405). Bioresour. Technol. **103**:293–299.
20. **Gerhardt P, Krieg NR, Murray RGE, Wood WA (ed).** 1994. Methods for general and molecular bacteriology. ASM Press, Washington, DC.
21. **Tolker-Nielsen T, Brinch UC, Ragas PC, Andersen JB, Jacobsen CS, Molin S.** 2000. Development and dynamics of *Pseudomonas* sp. biofilms. J. Bacteriol. **182**:6482–6489.
22. **Jensen PD, Hardin MT, Clarke WP.** 2009. Effect of biomass concentration and inoculum source on the rate of anaerobic cellulose solubilization. Bioresour. Technol. **100**:5219–5225.
23. **Bayer EA, Lamed R.** 1986. Ultrastructure of the cell surface cellulosome

of *Clostridium thermocellum* and its interaction with cellulose. J. Bacteriol. **167**:828–836.
24. **Bubner P, Dohr J, Plank H, Mayrhofer C, Nidetzky B.** 2012. Cellulases dig deep: in situ observation of the mesoscopic structural dynamics of enzymatic cellulose degradation. J. Biol. Chem. **287**:2759–2765.
25. **Weimer PJ, Price NPJ, Kroukamp O, Joubert L, Wolfaardt GM, Van Zyl WH.** 2006. Studies of the extracellular glycocalyx of the anaerobic cellulolytic bacterium *Ruminococcus albus* 7. Appl. Environ. Microbiol. **72**:7559–7566.
26. **Morrison M, Miron J.** 2000. Adhesion to cellulose by *Ruminococcus albus*: a combination of cellulosomes and Pil-proteins? FEMS Microbiol. Lett. **185**:109–115.
27. **Wiegel J, Dykstra M.** 1984. *Clostridium thermocellum*: adhesion and sporulation while adhered to cellulose and hemicellulose. Appl. Microbiol. Biotechnol. **20**:59–65.
28. **Bester E, Edwards EA, Wolfaardt GM.** 2009. Planktonic cell yield is linked to biofilm development. Can. J. Microbiol. **55**:1195–1206.
29. **Hyun HH, Zeikus JG, Longin R.** 1983. Ultrastructure and extreme heat resistance of spores from thermophilic *Clostridium* species. J. Bacteriol. **156**:1332–1337.
30. **Gould GW, Dring GJ.** 1975. Heat resistance of bacterial endospores and concept of an expanded osmoregulatory cortex. Nature **258**:402–405.
31. **Steiner E, Scott J, Minton NP, Winzer K.** 2012. An *agr* quorum sensing system that regulates granulose formation and sporulation in *Clostridium acetobutylicum*. Appl. Environ. Microbiol. **78**:1113–1122.
32. **Wuster A, Babu MM.** 2008. Conservation and evolutionary dynamics of the *agr* cell-to-cell communication system across firmicutes. J. Bacteriol. **190**:743–746.
33. **Burrell PC.** 2006. The detection of environmental autoinducing peptide quorum-sensing genes from an uncultured *Clostridium* sp. in landfill leachate reactor biomass. Lett. Appl. Microbiol. **43**:455–460.
34. **Sauer U, Santangelo JD, Treuner A, Buchholz M, Durre P.** 1995. Sigma factor and sporulation genes in *Clostridium*. FEMS Microbiol. Rev. **17**: 331–340.
35. **Yang B, Dai Z, Ding SY, Wyman CE.** 2011. Enzymatic hydrolysis of cellulosic biomass. Biofuels **2**:421–450.
36. **Zhang YP, Lynd LR.** 2004. Toward an aggregated understanding of enzymatic hydrolysis of cellulose: noncomplexed cellulase systems. Biotechnol. Bioeng. **88**:797–824.
37. **Strobel HJ.** 1995. Growth of the thermophilic bacterium *Clostridium thermocellum* in continuous culture. Curr. Microbiol. **31**:210–214.
38. **Strobel HJ, Caldwell FC, Dawson KA.** 1995. Carbohydrate transport by the anaerobic thermophile *Clostridium thermocellum* LQRI. Appl. Environ. Microbiol. **61**:4012–4015.
39. **Wells JE, Russell JB, Shi Y, Weimer PJ.** 1995. Cellodextrin efflux by the cellulolytic ruminal bacterium *Fibrobacter succinogenes* and its potential role in the growth of nonadherent bacteria. Appl. Environ. Microbiol. **61**:1757–1762.
40. **Lynd LR, Weimer PJ, Van Zyl WH, Pretorius IS.** 2002. Microbial cellulose utilization: fundamentals and biotechnology. Microbiol. Mol. Biol. Rev. **66**:506–577.
41. **Lamed R, Lobos J, Su T.** 1988. Effects of stirring and hydrogen on fermentation products of *Clostridium thermocellum*. Appl. Environ. Microbiol. **54**:1216–1221.
42. **Weimer PJ, Zeikus JG.** 1977. Fermentation of cellulose and cellobiose by *Clostridium thermocellum* in the absence and presence of *Methanobacterium thermoautotrophicum*. Appl. Environ. Microbiol. **33**:289–297.
43. **Guedon E, Payot S, Desvaux M, Petitdemange H.** 1999. Carbon and electron flow in *Clostridium cellulolyticum* grown in chemostat culture on synthetic medium. J. Bacteriol. **181**:3262–3269.
44. **Islam R, Cicek N, Sparling R, Levin D.** 2006. Effect of substrate loading on hydrogen production during anaerobic fermentation by *Clostridium thermocellum* 27405. Appl. Microbiol. Biotechnol. **72**:576–583.
45. **Berberich JA, Knutson BL, Strobel HJ, Tarhan S, Nokes SE, Dawson KA.** 2000. Product selectivity shifts in *Clostridium thermocellum* in the presence of compressed solvents. Ind. Eng. Chem. **39**:4500–4505.
46. **Rydzak T, Levin DB, Cicek N, Sparling R.** 2011. End-product induced metabolic shifts in *Clostridium thermocellum* ATCC 27405. Appl. Microbiol. Biotechnol. **92**:199–209.